Mo addition for improved electrochromic properties of V2O5 thick films

Issam Mjejri, Manuel Gaudon, Aline Rougier

Mo Addition for Improved Electrochromic Properties of V_2O_5 Thick Films

Issam Mjejri, Manuel Gaudon and Aline Rougier*

CNRS, Univ. Bordeaux, Bx INP, ICMCB, UMR 5026, F-33600 Pessac, France
*Corresponding Author: aline.rougier@icmcb.cnrs.fr, ICMCB-CNRS, 87 avenue du Dr Albert Schweitzer, 33608 Pessac cedex, France

Keywords: Polyol synthesis; Vanadium oxide; Electrochromism; Mo-Doping; Device.

Abstract:

Transition metal oxides (TMOs) have attracted considerable attention due to their variety of chromogenic properties. Among them, vanadium pentoxide (V_2O_5) has gained significant interest in respect of multichromism associated with orange, green and blue colors. Herein, we report a simple and easy method for the fabrication of Mo doped V_2O_5 thick films, leading to improved cyclability. Molybdenum doped vanadium pentoxide powders were synthesized from one single polyol route through the precipitation of an intermediate precursor: molybdenum doped vanadium ethyleneglycolate (Mo doped VEG). The as-synthesized Mo-doped V_2O_5 exhibits improved electrochromic performance in terms of capacity, cycling stability, and color contrast compared to single-component V_2O_5 in lithium as well as sodium based electrolyte. The improvement in EC performances lies in films of higher porosity as well as higher diffusion coefficients. To conclude, an electrochromic device combining Mo-V_2O_5 to $WO_3.2H_2O$, via a PMMA-lithium based electrolyte membrane exhibit simultaneously reversible color change from yellow to green for Mo-V_2O_5 and from blue to yellow white for $WO_3.2H_2O$ with a cycling stability up to 10 000 cycles.

I. Introduction

Today, the most promising technologies for lifetime efficiency and improved reliability include the use of smart materials [1-4]. For the latter, understanding and controlling of their

composition and microstructure are the ultimate objectives for improved properties. Smart materials are able to respond to stimuli and environmental changes and to activate their functions according to these changes [5]. The stimuli like temperature, pressure, light, electric flow, etc can originate internally or externally and lead to chromogenic materials described as thermochromic, piezoelectric, photochromic and electrochromic materials [6].

Electrochromism is the ability of materials and devices to change their optical properties when a voltage is applied [7-10]. The applications of electrochromic devices, ECDs, are multifold from smart windows in cars, rear-view mirrors and protective eyewear as transmittive or reflective properties and visible or infrared domain are concerned [11-15]. Among varieties of electrochromic materials, transition metal oxides (TMOs) are of growing interest because of their chemical stability in many electrolytes and nice reversible color switching [16-18]. Another advantageous specificity lies in the facility to improve the electrochromic properties by single or double doping or by addition of other materials and formation of composites [19-22]. Doping of material in electrochromic host lattice is expected to benefit the coloration efficiency and durability of the host, extending the switching potential range, and enhancing the reaction kinetics [23, 24].

Among varieties of TMOs, V_2O_5 has been receiving immense attention over the last decades due to properties such as electrochromism, and mixed electronic/ionic conduction, which give rise to applications in the field of optical displays and batteries [25-29]. The reversible intercalation of Na^+ or Li^+ cations into the V_2O_5 bilayer structure accompanied by a reduction of V^{5+} to V^{4+} is the common base for most of these properties.

Vanadium pentoxide is a good candidate for electrochromic device [10]. However, this oxide generally suffers from low conductivity, and stability during cycling. To solve this issue, considerable strategies have been proposed, such as reducing particle size, pore engineering, and modification by doping or coating to improve their stability and electronic conductivity

[30, 31]. Moreover, it has been demonstrated that the mixed-valence vanadium (molybdenum) oxides can provide readily accessible redox couples, which make them attractive for reversible delithiation/lithiation and also greatly shorten the transport path lengths of lithium ions and electrons during the delithiation/lithiation processes, thus leading to a significant improvement of the electrochemical performance [32-34]. There are several reports on the titanium, niobium and molybdenum doped V_2O_5 films deposited by different techniques [35, 36]. Shankara S. Kalanur et al. [30] have reported that the mixed MoO_3-V_2O_5 films exhibited better electrochromic properties compared to undoped V_2O_5 films. Granqvist [37] have demonstrated that the addition of Ti significantly promotes the amorphous nature of the films and stabilizes their electrochemical cycling performance and dynamic range for electrochromism. In our group, we have recently developed a single synthesis route named polyol process that leads to easy doping for tunable properties. Using this approach, Salek and al., [38] started modifying the electrochromic properties of V_2O_5 by doping with titanium. Indeed, polyol approach is one of the most promising methods for manufacturing materials with various morphologies and various structure-sensitive properties; this method is also environmentally friendly, economic, and easy to be implemented and allows the introduction of a large quantity of dopants [39-43]. In this study, we demonstrate the effect of molybdenum doping by polyol method on the electrochromic properties of vanadium pentoxide thick films by doctor blading deposition.

II. Experimental details

II.1. Molybdenum-doped vanadylglycolate salt (Mo-doped VEG) and Molybdenum-doped vanadium pentoxide (Mo-doped V_2O_5) powder

Molybdenum-doped vanadylglycolate (Mo-doped VEG) was synthesized by polyol process. Sodium molybdate (Na_2MoO_4, Aldrich) and ammonium-metavanadate (NH_4VO_3, Aldrich) were added in a round flask equipped with a reflux column and dissolved in various proportions (with Mo/(Mo+V) ratio varying between 0 and 20 mol %) in ethylene glycol ($H_6C_2O_2$). The

total cation metal concentration in EG was 0.1 M. The temperature of the reactive medium was increased slowly up to 160 °C under continuous stirring. After the complete dissolution of the precursor salt occurring at about 120 °C, the reflux was left to operate at 160 °C during 1 h to induce the complete coprecipitation. The precipitate was then separated by centrifugation and washed several times with ethanol and then dried at 80 °C for 10 h.

Mo-doped V_2O_5 powders were obtained by annealing Mo-doped VEG at 500 °C for 2 h under air atmosphere.

II.2. Characterization tools on undoped V_2O_5 and Mo-doped V_2O_5 powder/film

The powder structure was characterized by X-ray diffraction analysis (Philips PW 1820, PANalytical X'Pert instrument, 2θ range from 9 to 41° and $\lambda_{CuK\alpha1}$=1.54056 Å). Transmission electron microscopy (TEM) images were recorded with JEOL JSM-6700F (operating at 5 kV) microscope. ICP measurements allow the determination of the Mo/(Mo + V) molar ratio of the Mo-doped V_2O_5 powder samples. Measurements were carried out on aqueous solutions obtained after complete dissolution of the powder into HCl with high purity using the Varian ICP-OES 720ES apparatus.

Undoped V_2O_5 and Mo-doped V_2O_5 thick films were deposited by doctor blading method from homemade powders on ITO-coated (In_2O_3:Sn) glass (commercialized by SOLEMS with a resistance of 30Ω.□$^{-1}$). The thickness of the Mo-doped V_2O_5 thick films, measured using a Dektak mechanical profilometer, was of about 1.4 ± 0.1μm. For the identification of the crystal phases of the thick films, X-ray diffraction (XRD, Philips PW 1820, PANalyticalX ′Pert instrument, 2θ range from 10° to 50°and Cu $K_{\alpha1}\lambda$ = 0.154 056 nm) was used. The morphology and the elemental composition of the films were studied by SEM and EDS studies using a JEOL JSM-840 (operating at 15 kV) microscope.

II.3. Electrochromic measurements of undoped and Mo- doped vanadium pentoxides thick films

Electrochemical measurements were carried out in a three electrodes cell configuration using a BioLogic SP50 potentiostat/galvanostat apparatus and V_2O_5/Mo-V_2O_5 films on ITO/glass as working electrode. The counter-electrode and reference electrode consisted of a platinum foil and Saturated Calomel Electrode, SCE (E_{SCE} = 0.234 V/ENH), respectively. The operating voltage was controlled between -1.2 V and 2 V at 20 mV/s in both lithium- and sodium-based electrolytes, namely, lithium bis-trifluoromethane-sulfonimide (LiTFSI, Solvionic, purity > 99.99%) in ethylimidazoliumbis-(trifluoromethane-sulfonyl)-imide (EMITFSI) and sodium bis-trifluoromethane-sulfonimide (LiTFSI, Solvionic, purity > 99.99%) in ethylimidazoliumbis-(trifluoromethane-sulfonyl)-imide (EMITFSI). All the electrochemical measurements were performed at room temperature.

The diffuse reflectance of undoped V_2O_5 and Mo-doped V_2O_5 films were *ex situ* recorded after application of various potentials using a Varian Cary 5000 UV-Vis-NIR spectrophotometer.

II.4. Fabrication of Electrochromic Device

Using the common 5-layer-type battery device, an electrochromic device consisting of two inorganic electrochromic films separated by an electrolyte was assembled. Mo-V_2O_5 and $WO_3.2H_2O$ were employed as the two electrodes, and the LiTFSI-EMTFSI blended with PMMA (Solvionic) was used as the electrolyte membrane. The two electrodes were prepared from homemade powders synthesized by polyol process and deposited by doctor blading.

III. Results and discussion

III.1. Powders

As introduced in the experimental section, the synthesis of Mo-doped V_2O_5 results from a two steps process (i) coprecipitation of the Mo-doped VEG and (ii) annealing of the Mo-VEG at 500 °C under air atmosphere leading to Mo-doped V_2O_5.

At first glance, the X-ray patterns of Mo:VEG obtained by coprecipitation show no significant modification (Figure 1) up to 20 mol % of molybdenum. All the X-ray peaks are indexed in the VEG phase (00-049-2497 JCPDS data file; C2/c space group), indicating that Mo ions may be incorporated into the bulk of the VEG without destroying its original structure while a decrease in the XRD peak intensity with gradual Mo doping suggests a progressive amorphization.

The slight decrease of the half widths with increasing Mo concentration is associated with a decrease of the average crystallite size of the precipitated glycolate Mo-VEG, as calculated from Scherrer formula (Table 1).

The X-ray diffraction patterns of the V_2O_5 and Mo-V_2O_5 powders after annealing the VEG at 500 °C under air for 2 h (Figure 2) exhibit well-resolved diffraction peaks indexed in an orthorhombic phase (00-041-1426 JCPS file; Pmnm space group). Up to 10 mol % of Mo, only a slight increase in the width of the XRD peaks is detected while a new peak located at 29.9 ° appears for 20 % of Mo. This peak could be identified as the 100 % intensity of a molybdenum rich impurities (MoO_3 type hexagonal phase).

TEM images of the undoped and doped V_2O_5 powders show in first approximation that the oxides consist of nanometric crystallites aggregated in packs (Figure 3). Besides, with Mo addition, a second morphology consisting of batonnets with hexagonal section starts to be visible and becomes more prominent for the 20 % Mo concentration (Fig. 3, b, c, d).

From ICP measurements made on doped samples, the evolution of the efficient molybdenum concentration versus the target one can be described by an affine function $y = ax + b$ with $a = 0.19$ and $b = -0.17$ indicating that the real rate is different from the target one (Figure 4). Indeed, for 20 % mol of Mo target rate, only 3.6 % are really introduced.

In the following aiming at studying the EC properties of pure phase, attention is focused on the 10 % Mo doped V_2O_5 corresponding of 1.9 % real rate of Mo in the powder. However, for simplicity, we use the target rate of 10 %.

III.2. Films

III.2.1. Electrochromic properties in lithium based electrolyte

Thick films of undoped and Mo-doped V_2O_5 (1.4 μm) were deposited by doctor blade and their EC properties were evaluated through cyclic voltammetry carried out in ionic liquid electrolyte. The cyclic voltammograms, CVs, of the undoped (-0.9 V - 1.9 V) and Mo-doped V_2O_5 (-1.2 V – 1.9 V) films are shown in Figure 5 a. The CVs of Mo-V_2O_5 films exhibit a higher current density compared to undoped V_2O_5 samples corresponding to higher electrochemical capacity Q (recorded in oxidation) of 65 mC/cm^2 versus 55 mC/cm^2 for undoped V_2O_5. Upon cycling the influence of Mo on the capacity becomes even more visible as the capacity for Mo-V_2O_5 film increases while the one of V_2O_5 decreases (Fig. 5b). After 500 cycles, the V_2O_5 capacity has decreased from about 10 % of its initial capacity while Mo-V_2O_5 films exhibits an opposite behavior with an increase in capacity of about 15% (75mC/cm^2 for Mo:V_2O_5 is recorded as compared to ~ >Q 45 mC/cm^2 for V_2O_5). Upon cycling, both films exhibit multi-chromism from orange (1.9 V) to green (-0.3 V) and blue (-0.9 V) (Fig. 5 c).

A simple assumption to explain the increase in stability lies in the film morphology. Indeed, the comparison of the SEM images of V_2O_5 and 10% Mo-V_2O_5 shows for both films an uniform microstructure with however visible differences (Fig. 6).

From V_2O_5 nanopowders, doctor blading process induces the appearance of micrometric lamellar platelets of about 5 × 2 μm embedded in between small grains. With Mo addition, the film morphology appears more porous favoring a large surface exchange with the electrolytes that could explain the higher capacity recorded for the Mo-V_2O_5 films (Fig. 5b). EDX elemental mapping confirms the Mo homogeneous distribution (Supporting Information S1). The XRD

patterns of the opaque film deposited on ITO substrate are presented in Figure 7. All the diffraction peaks match the ones of the orthorhombic crystalline phase (JCPDS# 00-041-1426) and of the ITO substrate (JCPDS # 44-1087). Besides, as observed for un-doped V_2O_5 preferential orientation along the (001) crystallographic direction is clearly detected [44].

Further cycling of the Mo-V_2O_5 films up to 1000 cycles (Fig. 8a) confirms their good reversibility and stability associated with nice optical switch in between a reduced blue state (−1.2 V) and an oxidized orange state (+1.9 V) associated with reflectance values of less than 4 % and of 60 % at 610 nm, respectively, leading to an optical reflectance modulation, ΔR, of about 55% (Fig. 8b).

In CIE colorimetric space, the color is represented by three parameters, the luminance axis (L*) and two hue axes (a*) and (b*), which can be used to define and compare quantitatively the colors. The relative luminance (L*), the hue (a*) and (b*) values of Mo-V_2O_5 films in different states were determined. Indeed, for the blue-reduced state (at −1.2 V), the L*a*b* parameters are 24, −13, and -6, respectively, whereas for the orange-oxidized state (at +1.9 V), the L*a*b* parameters are 78, 14, and 35, respectively. The contrast $\Delta E^* = [(L^*_2 - L^*_1)^2 + (a^*_2 - a^*_1)^2 + (b^*_2 - b^*_1)^2]^{1/2}$ is 73.

As shown in Figure 9a, a decrease in scan rate from 50 to 5 mV/s is associated with a progressive evolution of the CV shape corresponding to the appearance of peaks, of which resolution increases (Fig. 9a). The symmetrical aspect of the redox peaks confirms the good electrochemical reversibility. For an increase in scan rate to 50 mV/s (Fig. 9a), the cathodic and anodic peak currents increase simultaneously. The anodic and cathodic maximum current density (j_a) and (j_c) exhibits a linear relation with the square root of scanning rate ($V^{1/2}$) (Fig. 9b and c). The peak current density is proportional to $V^{½}$ which may indicate a diffusion-controlled process. The diffusion coefficient D of lithium ions (Li^+) was calculated using Randles-Sevcik equation [31, 45]:

$$J_a = 2*69\ 10^5\ n^{3/2} A\ D^{1/2}\ C\ v^{1/2}$$

Where j_a is the anodic maximum current density at oxidation state, n is the number of electrons transferred, A is the electrode area (cm^2), D is the diffusion coefficient (cm^2/s), C is the concentration of the electrolyte (mol/cm^3), and v is the voltage scan rate (V/s). The linear relation is expected for a diffusion-controlled process allowing the determination of the diffusion coefficient, $D_{Li+} = 8.4*10^{-8}\ cm^2/s$.

This value is one order of magnitude higher than the diffusion coefficient obtained for the undoped V_2O_5 ($D_{Li+} = 6.1*10^{-9} cm^2/s$) [10] in agreement with a more visible porosity of the doped films and of their higher electrochemical capacity. The value remains much higher than the ones recorded in the literature [45, 46]. The origin of such difference is not clear but probably comes from the peculiar morphology of thick films doctor bladed from nanopowders.

III.2.2. Electrochromic properties in sodium-based electrolyte

The similarities in the materials and mechanisms occurring in the field of batteries and of electrochromic systems, also described as optical-batteries, have stimulated our interest for opening the characterization of the EC properties to sodium-based electrolytes. As a matter of fact, V_2O_5 has received significant attention for the challenging issues of Na-ion batteries [47]. On the contrary, to our knowledge its EC properties in Na electrolyte has been scarcely addressed and never for Mo doped V_2O_5. The electrochemical activity of the Mo-V_2O_5 films in a Li^+-based electrolyte, namely, LiTFSI-EMITFSI, was compared with the one in a Na^+-containing electrolyte, namely (Figure 10), NaTFSI-EMITFSI. The CVs of the Mo-V_2O_5 thick films in NaTFSI-EMITFSI electrolyte show a nice reversible behavior and a good cyclability up to 500 cycles nevertheless associated with a rather different CV shape with no visible peaks shortly described as the duck-shape (Supporting information S2). Upon extended cycling, the absence of even a minimal deviation from the anodic/cathodic peak position confirms the

absence of degradation and the good cyclability of Mo-doped V_2O_5 in both lithium and sodium based electrolytes. Upon cycling, the initially orange Mo-V_2O_5 films turns green at (-0.9 V) and then from green to orange at (+1.9 V) (Supporting information S3). When the scan rate increases to 50 mV/s (Supporting information S4), the cathodic and anodic peak currents increase simultaneously. The linear relationship of the anodic/cathodic peak current density ($j_{a,c}$) with the square root of scanning rate ($V^{1/2}$) (Supporting information S5) leads to the determination of the diffusion coefficient $D_{Na+} = 1.2*10^{-8}$ cm^2/s. The decrease in diffusion coefficient from Li to Na media well agrees with the decrease in the current density values. Such trend supports the fact that the redox processes are more difficult for larger cations than for small ones leading to favor capacitive surface phenomena as compared to insertion-deinsertion faradic process.

III.3. Electrochromic display

For assessing practical applications, ECD with double sided colored was constructed by combining Mo-V_2O_5 films to $WO_3.2H_2O$ ones. The description of the $WO_3.2H_2O$ films is summarized in supplementary information (Supporting information S6 and S7). The two films, individually deposited on an ITO substrate, were associated using a hydrophobic electrolyte membrane based of LiTFSI-EMITFSI with PMMA as an ion conductor. Prior to device assembly, the $WO_3.2H_2O$ thick film was cycled in LiTFSI-EMITFSI electrolyte for few cycles (Supporting information S8) and assembled in the blue reduced state to the precycled orange Mo-V_2O_5. The Mo-V_2O_5 and $WO_3.2H_2O$ films simultaneously change colors upon cycling Figure 11.

The durability of Mo-V_2O_5/electrolyte/ $Li_xWO_3.2H_2O$ device was studied by CV at the scan rate of 20 $mV{\cdot}s^{-1}$ in the -1.0 V − 1.9 V voltage window (Figure 12). The electrochemical stability of the Mo-V_2O_5/LiTFSI in EMITFSI +PMMA/ $Li_xWO_3.2H_2O$ proved to be excellent through 10 000 repeated cycles of oxidation and reduction showing even an increase of capacity

upon cycling. The good reversibility is associated with nice color switches which differ on the two faces, depending on whether Mo-V_2O_5 or $WO_3.2H_2O$ film is visible.

Mo-V_2O_5 reversibly changes from orange to dark-green and $WO_3.2H_2O$ from blue to yellow-white (Fig. 11). The color switching time was about 8 s upon reduction (green/white) and 5 s upon oxidation (orange/blue).

Figure 13 shows the *in-situ* optical reflectance spectra for the reduced and oxidized states from the double-sided EC device recorded on each side. The reduced green state (−1.5 V/60 s) and the oxidized orange state (+1.5 V/60 s) (Fig. 13 a) are associated with reflectance values of about $R_R \approx 13\%$ and $R_O \approx 27\%$ at 600 nm, respectively, corresponding to a reflectance modulation ΔR of 14 %. The *in-situ* evolution of the reflectance spectra for the second face ($WO_3.2H_2O$) is depicted in Figure 13 b. The blue state (+1.5 V/60 s) and the oxidized-white state (-1.5/60 s) are associated with reflectance values of about $R_R \approx 7\%$ and $R_O \approx 15\%$ at 500 nm, respectively, with a total reflectance modulation of $\Delta R \approx 8\%$.

The optical contrasts of the two faces were evaluated using the CIE L*a*b* color system. The simultaneous switching from orange to green for Mo-V_2O_5 side, and from blue to yellow-white for $WO_3.2H_2O$ side, corresponds to ΔE^* of the order of 45 and 29, respectively.

IV. Conclusion

In this paper, we demonstrate improved electrochromic properties for doctor bladed Mo doped V_2O_5 thick films cycled in lithium-based electrolyte. Higher electrochemical capacity and stability are correlated to an increase in film porosity as well to an increase in ionic coefficient value with Mo addition. The interesting EC properties are extended to sodium based electrolyte, highlighting the suitable use in both Li and Na media. To conclude, the EC properties are

confirmed in a double-sided EC device combining blue-green-orange Mo-V_2O_5 films to blue-white $Li_xWO_3.2H_2O$ film. This work is a further step in our investigation of thick films integrated in EC device with unusual double–sided configuration aiming at addressing new applications in decorative field for instance.

Acknowledgments:

The authors thank Alexandre Fargues (ICMCB) for the optical measurements, Laetitia Etienne (ICMCB) for the ICP measurements and Marion Gayot (CNRS, Université de Bordeaux, PLACAMAT UMS 3626) for the TEM images.

REFERENCES

[1] C. G. Granqvist, P. C. Lansåker, N. R. Mlyuka, G. A. Niklasson, E. Avendaño, Progress in Chromogenics: New Results for Electrochromic and Thermochromic Materials and Devices. Sol. Energy Mater. Sol. Cells 93 **(2009)** 2032–2039.

[2] A. Samy, Y. Mohamed, Smart Materials Innovative Technologies in Architecture; Towards Innovative Design Paradigm. Energy Procedia 115 **(2017)** 139-154.

[3] J. Oliveira, V. Correia, H. Castro, P. Martins, S. Lanceros-Mendez, Polymer-based Smart Materials by Printing Technologies: Improving Application and Integration. Additive Manufacturing 21 **(2018)** 269-283.

[4] Y. Lu, X. Xiao, J. Fu, C. Huan, S. Qi, Y. Zhan, Y. Zhu, G. Xu, Novel Smart Textile with Phase Change Materials Encapsulated Core-Sheath Structure Fabricated by Coaxial Electrospinning. Chemical Engineering Journal 355 **(2019)** 532–539.

[5] W.-G. Drossel, F. Meinel, A. Bucht, H. Kunze, Smart Materials for Smart Production –a Cross-Disciplinary Innovation Network in the Field of Smart Materials. Procedia Manufacturing 21 **(2018)** 197–204.

[6] A. Avenda, A. Azens, G.A. Niklasson, C.G. Granqvist, Sputter Deposited Electrochromic Films and Devices Based on These: Progress on Nickel-Oxide-Based Films. Mater. Sci. Eng. B 138 **(2007)** 112–117.

[7] A. A. Argun, P. H. Aubert, B. C. Thompson, I. Schwendeman, C. L. Gaupp, J. Hwang, N. J. Pinto, D. B. Tanner, A. G. M. Diarmid, J. R. Reynolds, Multicolored Electrochromism in Polymers: Structures and Devices. Chem. Mater., 16 **(2004)** 4401-4412.

[8] C. J. Barile, D. J. Slotcavage, M. D. McGehee. Polymer−Nanoparticle Electrochromic Materials that Selectively Modulate Visible and Near-Infrared Light. Chem. Mater, Chem. Mater., 28 **(2016)** 1439–1445.

[9] R. J. Mortimer, A. L. Dyer, J. R. Reynolds, Electrochromic Organic and Polymeric Materials for Display Applications. Displays 27 **(2006)** 2–18.

[10] I. Mjejri, L.M. Manceriu, M. Gaudon, A. Rougier, F. Sediri, Nano-Vanadium Pentoxide Films for Electrochromic Displays. Solid State Ionics 292 **(2016)** 8–14.

[11] C. G. Granqvist, M.A. Arvizu, H.Y. Qu, R. T. Wen, G. A. Niklasson, Advances in Electrochromic Device Technology: Multiple Roads Towards Superior Durability. Surface Coatings Technology 357 **(2019)** 619-625.

[12] A. Danine, L. Cojocaru, C. Faure, C. Olivier, T. Toupance, G. Campet, A. Rougier, Room Temperature UV Treated WO_3 Thin Films for Electrochromic Devices on Paper Substrate. Electrochim. Acta 129 **(2014)** 113-119.

[13] I. Mjejri, C. M. Doherty, M. Rubio-Martinez, G. L. Drisko, A. Rougier, Double Sided Electrochromic Device Based on MetalOrganic Frameworks. ACS Appl. Mater. Interfaces 9 **(2017)** 39930- 39934.

[14] Z. Tong, J. Hao, K. Zhang, J. Zhao, B. L. Su, Y. Li, Improved Electrochromic Performance and Lithium Diffusion Coefficient in Three Dimensionally Ordered Macroporous V_2O_5 films. J. Mater. Chem. C 2 **(2014)** 3651-3658.

[15] C. G. Granqvist, Oxide Electrochromics: An Introduction to Devices and Materials. Sol. Energy Mater. Sol. Cells 99 **(2012)** 1−13.

[16] I. Mjejri, R. Grocassan, A. Rougier, Enhanced Coloration for Hybrid Niobium-Based Electrochromic Devices. ACS Appl. Energy Mater., 1 **(2018)** 4359−4366.

[17] D. H. Kim, Effects of Phase and Morphology on the Electrochromic Performance of Tungsten Oxide Nano-urchins. Sol. Energy Mater. Sol. Cells 107 **(2012)** 81–86.

[18] S. Hou, A.I. Gavrilyuk, J. Zhao, H. Geng, N. Li, C. Hua, K. Zhang, Y. Li, Controllable Crystallinity of Nickel Oxide Film with Enhanced Electrochromic Properties. Appl. Surf. Sci., 451 **(2018)** 104–111.

[19] M. A. Arvizu, G. A. Niklasson, C. G. Granqvist, Electrochromic $W_{1-x-y}Ti_xMo_yO_3$ Thin Films Made by Sputter Deposition: Large Optical Modulation, Good Cycling Durability, and Approximate Color Neutrality. Chem. Mater., 29 **(2017)** 2246−2253.

[20] S. Mishra, P. Yogi, P. R. Sagdeo, R. Kumar, TiO_2−Co_3O_4 Core−Shell Nanorods: Bifunctional Role in Better Energy Storage and Electrochromism. ACS Appl. Energy Mater., 1 **(2018)** 790−798.

[21] S. J. Lee, H. P. Kim, A. R. bin Mohd Yusoff, J. Jang, Organic Photovoltaic With PEDOT: PSS and V_2O_5 Mixture as Hole Transport Layer. Sol. Energy Mater. Sol. Cells 120 **(2014)** 238−243.

[22] H. Alhummiany, S. Rafique, K. Sulaiman, XPS Analysis of the Improved Operational Stability of Organic Solar Cells Using a V_2O_5 and PEDOT: PSS Composite Layer: Effect of Varied AtmosphericConditions.J. Phys. Chem. C 121 **(2017)** 7649−7658.

[23] S. Xie, Z. Bia, Y. Chena, X. Hea, X. Guo, X. Gao, X. Li, Electrodeposited Mo-Doped WO_3 Film With Large Optical Modulation and High Areal Capacitance Toward Electrochromic Energy-Storage Applications. Applied Surface Science 459 **(2018)** 774-781.

[24] V. Madhavi, P. J. Kumar, P. Kondaiah, O. M. Hussain, S. Uthanna, Effect of Molybdenum Doping on the Electrochromic Properties of Tungsten Oxide Thin Tilms by RF Magnetron Sputtering. Ionics 20 **(2014)** 1737–1745.

[25] M. Kovendhan, P. D. Joseph, P. Manimuthu, A. Sendilkumar, S. N. Karthick, S. Sambasivam, K. Vijayarangamuthu, H. J. Kim, B. C. Choi, K. Asokan, C. Venkateswaran, R. Mohan, Prototype Electrochromic Device and Dye Sensitized Solar Cell using Spray Deposited Undoped and 'Li' Doped V_2O_5 Thin Film Electrodes. Curr. Appl. Physics 15 **(2015)** 622−631.

[26] C. F. Armer, J. S. Yeoh, X. Li, A. Lowe, Electrospun Vanadium-Based Oxides as Electrode Materials. J. Power Sources 395 **(2018)** 414-429.

[27] J. Yao, Y. Li, R. C. Massé, E. Uchaker, G. Cao, Revitalized Interest in Vanadium Pentoxide as Cathode Materials for Lithium-ion Batteries and Beyond. Energy Storage Materials 11 **(2018)** 205-259.

[28] A. Talledo, C. G. Granqvist, Electrochromic VanadiumPentoxide-Based Films: Structural, Electrochemical, and Optical Properties. J. Appl. Phys., 77 **(1995)** 4655.

[29] I. Mjejri, A. Rougier, M. Gaudon, Low-Cost and Facile Synthesis of the Vanadium Oxides V_2O_3, VO_2, and V_2O_5 and Their Magnetic, Thermochromic and Electrochromic Properties. Inorg. Chem. 56 **(2017)** 1734−1741.

[30] S. S. Kalanur, H. Seo, Influence of Molybdenum Doping on the Structural, Optical and Electronic Properties of WO_3 for Improved Solar Water splitting. J. Colloid Inter. Sci., 509 **(2018)** 440-447.

[31] C.E. Patil, P.R. Jadhav, N.L. Tarwal, H.P. Deshmukh, M.M. Karanjkar, P.S. Patil. Electrochromic Performance of Mixed V_2O_5–MoO_3 Thin Films Synthesized by Pulsed Spray Pyrolysis Technique. Mater. Chem. Physics 126 **(2011)** 711–716.

[32] A. Jin, W. Chen, Q. Zhu, High Li^+-ion Storage Capacity and Multi-electrochromism Behavior of Electrodeposited Molybdenum Doped Vanadium Oxide Films. Advanced Mater. Res., 79-82 **(2009)** 799-802.

[33] W. Yong, H. L. Zhang, H. T. Cao, T. Tian, J. H. Gao, L. Y. Liang, F. Zhuge Effect of Post-annealing on Structural and Electrochromic Properties of Mo-doped V_2O_5 Thin Films. J Sol-Gel Sci Technol 77 **(2016)** 604-609.

[34] N. G. Prakash, M. Dhananjaya, B. P. Reddy, K. S. Ganesh, A. L. Narayana, O.M. Hussain, Molybdenum Doped V_2O_5 Thin Films Electrodes for Supercapacitors. Materials Today: Proceedings 3 **(2016)** 4076–4081

[35] S. K. Sinha, Effect of Temperature on Structural, Optical and Electrical Properties of Pulsed-laser Deposited W-doped V_2O_5 Thin Films. Superlattices Microstructures 125 **(2019)** 88-94.

[36] T. M. Westpha, C. M. Cholant, C. F. Azevedo, E. A. Moura, D. L. da Silva, R. M. J. Lemos, A. Pawlicka, A. Günde, W. H. Flores, C.O. Avellaned, Influence of the Nb_2O_5 Doping on the Electrochemical Properties of V_2O_5 Thin Films. J. Electro. Chem., 790 **(2017)** 50-56.

[37] M.A. Arvizua, C.A. Triana, B.I. Stefanov, C.G. Granqvist, G.A. Niklasson, Electrochromism in Sputter-Deposited W–Ti Oxide Flms: Durability Enhancement Due to Ti. Sol. Energy Mater. Sol. Cells 125 **(2014)** 184-189.

[38] G. Salek, B. Bellanger, I. Mjejri, M. Gaudon, A. Rougier, Polyol Synthesis of Ti-V_2O_5 Nanoparticles and Their Use as Electrochromic Films. Inorg. Chem. 55 **(2016)** 9838−9847.

[39] I. Mjejri, S. Mornet, M. Gaudon. From nano-structured polycrystalline spheres with $Zn_{1-x}Co_xO$ composition to core-shell $Zn_{1-x}Co_xO@SiO_2$ as green pigments. J. Alloys Compd. **777 (2019)** 1204-1210.

[40] S. Guan, M. Gaudon, M. Souquet-Basiège, O. Viraphong, N. Penin, A. Rougier, Carbon-reduction as an easy route for the synthesis of VO_2(M1) and further Al, Ti doping, Dalton Trans., 48 **(2019)** 3080-3089.

[41] H. Grisaru, O. Palchik, A. Gedanken, V. Palchik, M. A. Slifkin, A. M. Weiss, Y. Rosenfeld Hacohen. Preparation of $Cd_{1-x}Zn_xSe$ Using Microwave-Assisted Polyol Synthesis. Inorg. Chem. 40 **(2001)** 4814-4815.

[42] H. J. Han, T. Yu, W. S. Kim, S. H. Im. Highly reproducible polyol synthesis for silver nanocubes. Journal of Crystal Growth, 469 **(2017)** 48-53.

[43] W. B. Soltan, M. Mbarki, S .Ammar, O. Babot, T. Toupance. Structural and optical properties of vanadium doped SnO_2 nanoparticles synthesized by the polyol method. Optical Materials, 54 **(2016)** 139-146.

[44] I. Mjejri, M. Gaudon, G. Song, C. Labrugère, A. Rougier, Crystallized V_2O_5 as Oxidized Phase for Unexpected Multicolor Electrochromism in V_2O_3 Thick Film. ACS Appl. Energy Mater., 1 **(2018)** 2721−2729.

[45] C. M. Cholant, C. F. Azevedo, I. Caldeira, R. D. C. Balboni, E. A. Moura, T. M. Westphal, A. Pawlicka, M. A. C. Berton, J. A. Gomez, C. O. Avellaneda, Li^+ Ions Diffusion Coefficient in V_2O_5:MoO_3 Sol-Gel films. Molecular Crystals and Liquid Crystals, 655 **(2017)** 61-70.

[46] Z. Tong, J. Hao, K. Zhang, J. Zhao, B-L. Su, Y. Li, Improved electrochromic performance and lithium diffusion coefficient in three-dimensionally ordered macroporous V_2O_5 films J. Mater. Chem C 2 **(2014)** 3651–3658.

[47] E. Adamczyk, M. Gnanavel, V. Pralong, Redox Activity of Sodium Vanadium Oxides towards Oxidation in Na Ion Batteries. Materials 11 **(2018)** 1021.

Table 1. Estimation of the crystallite size using the Scherrer formula for Mo-VEG with different Mo concentrations from 0 to 20 %

Sample	Grain size (nm)
Pure VEG	80
5% Mo doped VEG	65
10% Mo doped VEG	59
20% Mo doped VEG	34

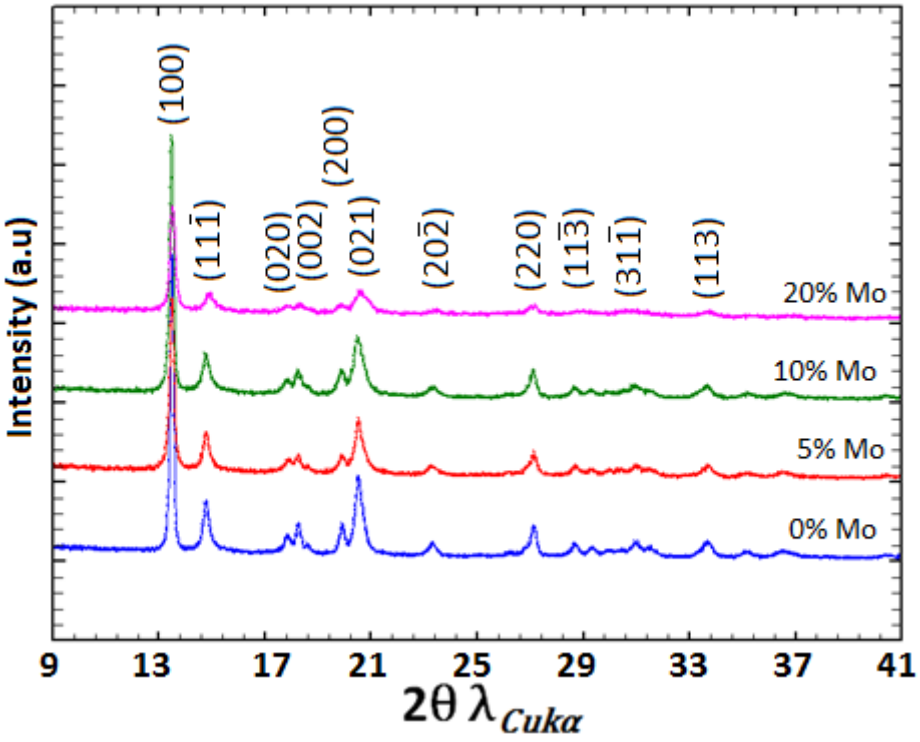

Fig. 1. X-ray diffraction patterns of the precipitate (Mo-VEG) obtained from polyol synthesis for various Mo/(Mo + V) mol %. Peak indexation is made using the 00-049-2497 JCPDS data file; C2/c space group.

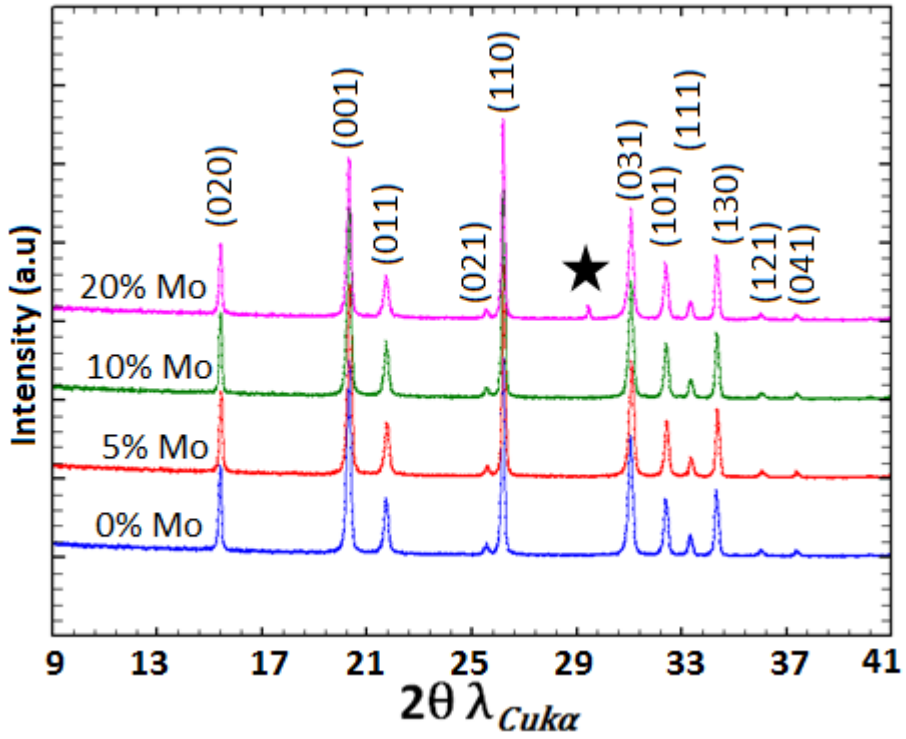

Fig. 2. X-ray diffraction patterns of Mo-doped V_2O_5 powders after a thermal treatment at 500 °C under air for 2 h. Peak indexation is made using the 00-041-1426 JCPS file; Pmnm space group.

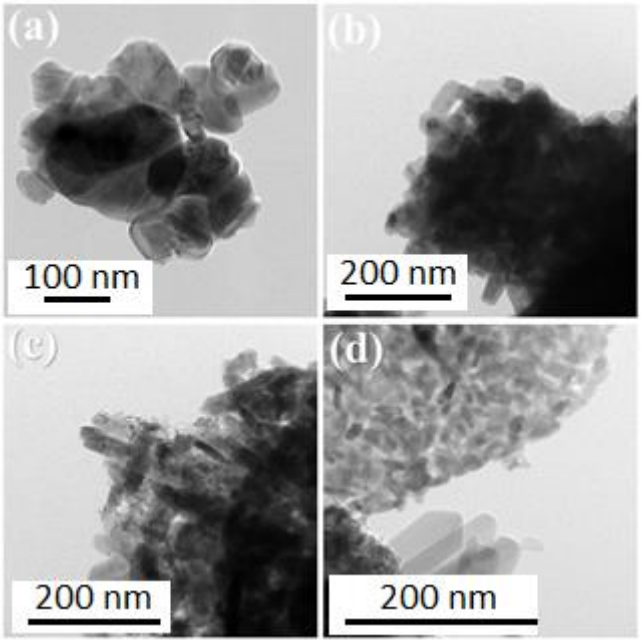

Fig. 3. TEM images of (a) undoped V_2O_5, (b) V_2O_5 doped with 5% Mo, (c) V_2O_5 doped with 10% Mo and (d) V_2O_5 doped with 20% Mo.

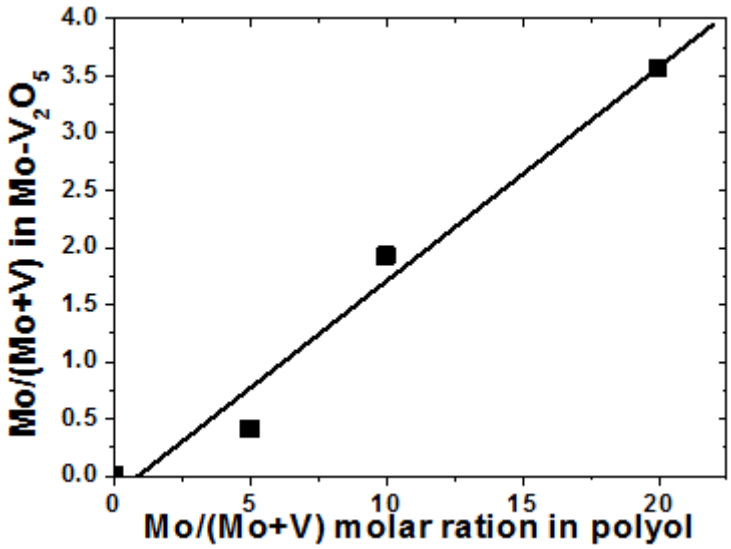

Fig. 4. Mo/(Mo + V) molar ratio determined by ICP in Mo-doped V_2O_5 versus the introduced ratio in the ethylene glycol bath.

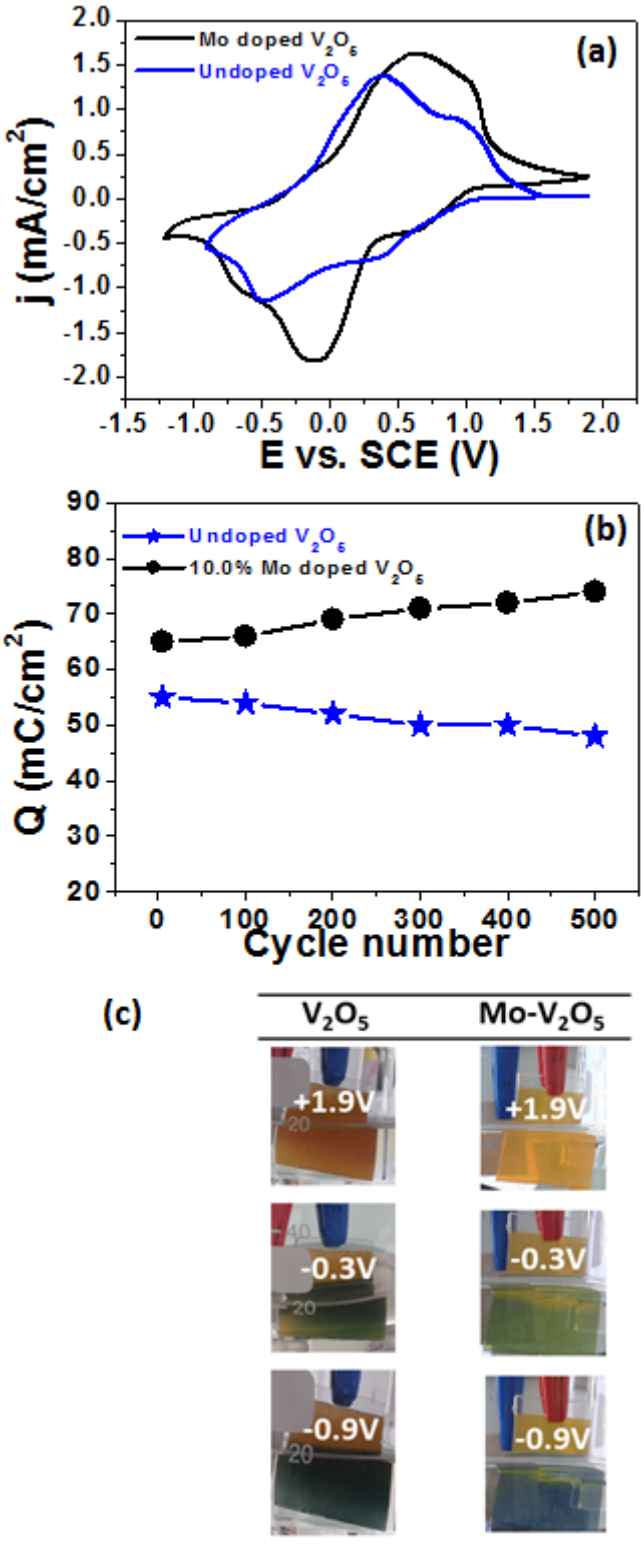

Fig. 5. Comparison of 2nd Cyclic Voltammograms of undoped V_2O_5 and 10% Mo doped V_2O_5 (a). The films are cycled in Mo-V_2O_5 (V_2O_5)/LiTFSI in EMITFSI/Pt vs SCE cells with a scan rate of 20 mV/s. Evolution of the electrochemical capacity of undoped V_2O_5 compound and V_2O_5 doped with 10% Mo (b). Visual appearance, orange (+1.9 V) and two distinct reduced states (−0.3 V (greenish) and −0.9 V (bluish)) (c). (For interpretation of the references to color in this figure legend, the reader is referred to the Web version of this article.)

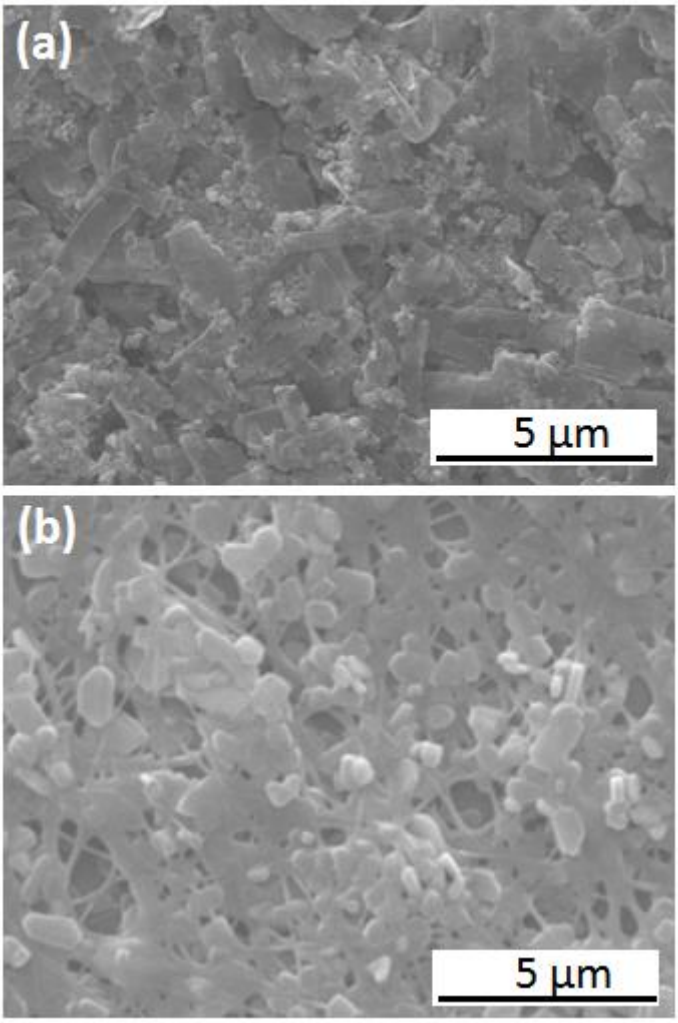

Fig. 6. SEM patterns of (a) pure V_2O_5 and (b) 10% Mo doped V_2O_5 films.

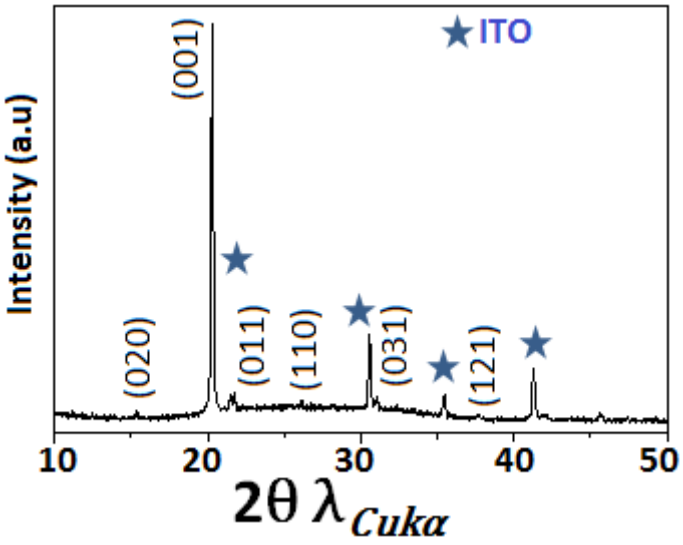

Fig. 7. XRD patterns of the V_2O_5 doped with 10% Mo films deposited on ITO/glass substrate.

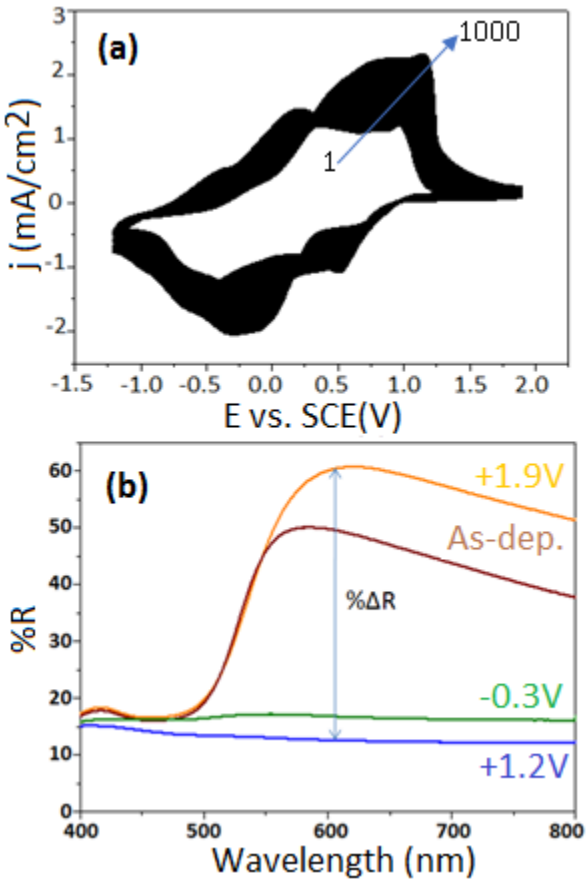

Fig. 8. Electrochromic properties of Mo-V_2O_5 in LiTFSI in EMITFSI and (b) corresponding *ex situ* diffuse reflectance spectra for the 10% Mo doped V_2O_5 films cycled in LiTFSI in EMITFSI after 1000 cycles, brownish curve for as-deposited state, green and blue are the two reduced states at (−0.3 V and −1.2 V) and re-oxidized orange state at (+1.9 V). (For interpretation of the references to color in this figure legend, the reader is referred to the Web version of this article.)

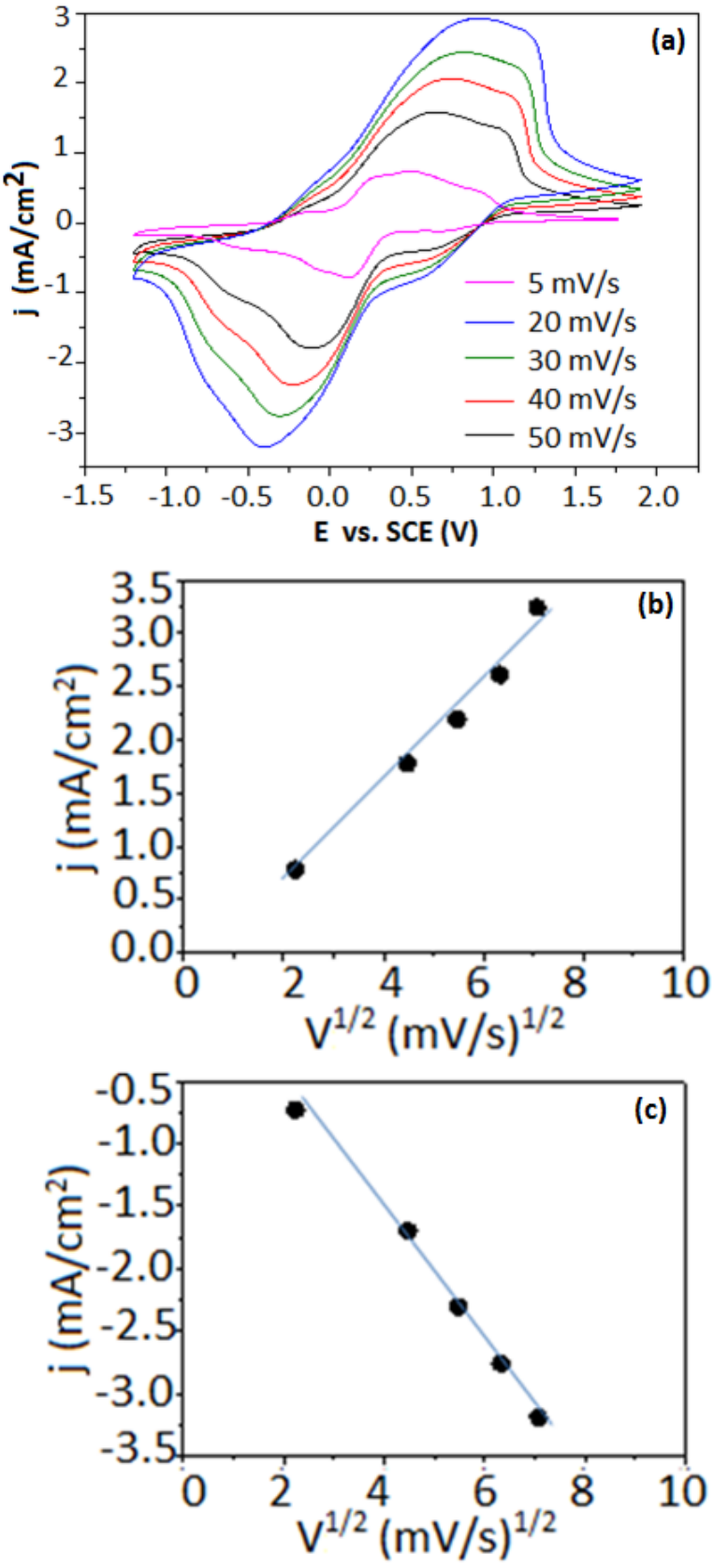

Fig. 9. Cyclic voltammograms of (a) Mo-V_2O_5 film in LiTFSI in EMITFSI at different scan rates, (b) anodic current density vs. $v^{1/2}$ and (c) cathodic current density vs. $v^{1/2}$.

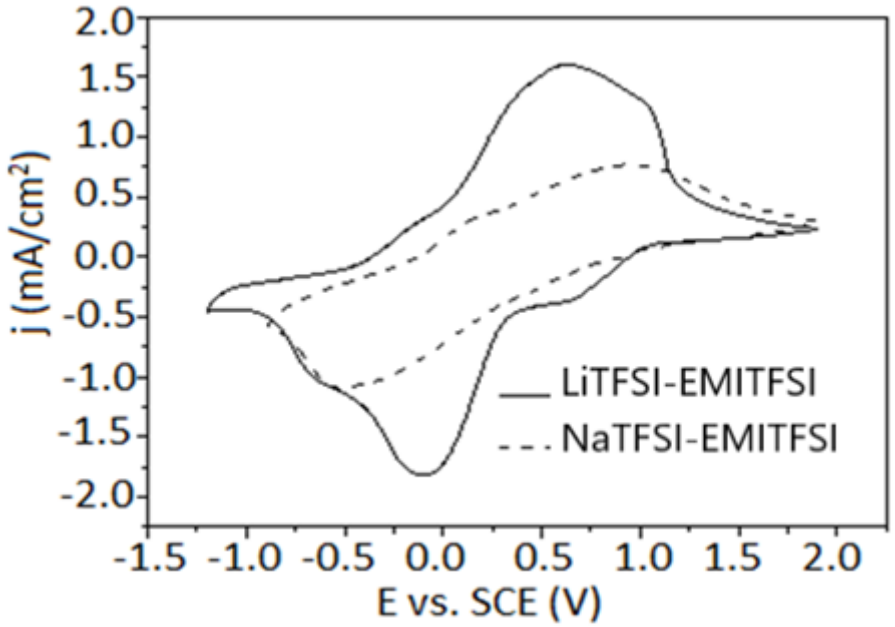

Fig. 10. Comparison of cyclic voltammograms of the Mo-V_2O_5 films in LiTFSI-EMITFSI (solid line) and in NaTFSI-EMITFSI (dash line) electrolyte in three electrodes cell.

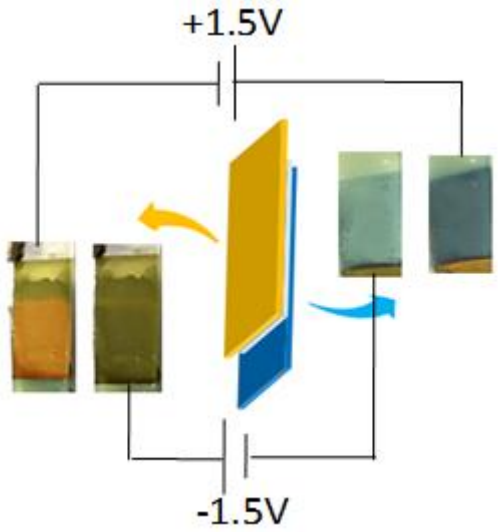

Fig. 11. Photo of the device in the reduced and oxidized state at the −1.5/60 s to 1.5 V/60 s.

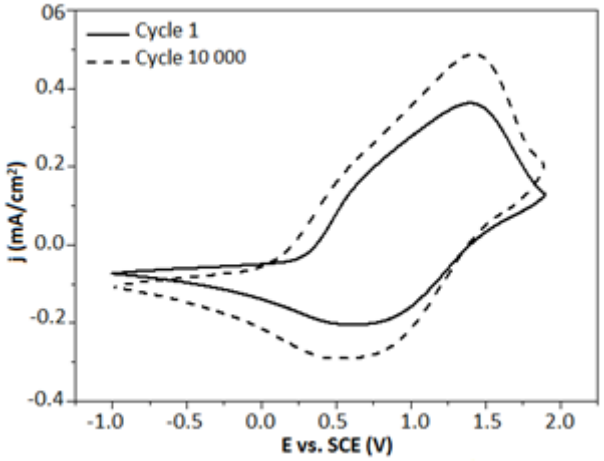

Fig. 12. (a) Cyclic voltammograms of the ITO/Mo-V_2O_5/LiTFSI in EMITFSI + PMMA/$Li_xWO_3.2H_2O$ device /ITO device between −1 and + 1.9 V with a 20 mV/s scan rate up to 10 000 cycles.

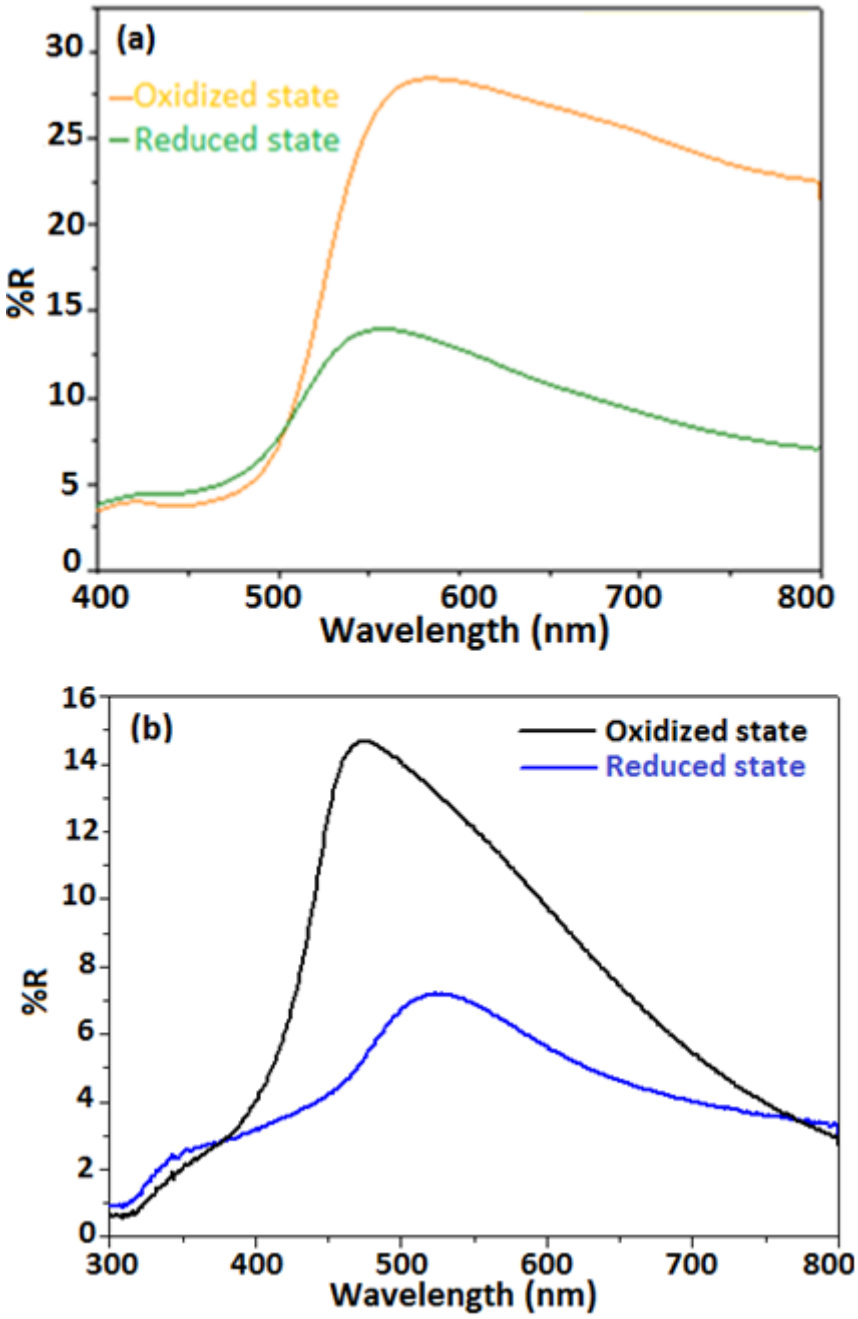

Fig. 13. *In-situ* diffuse reflectance spectra of the Mo-V_2O_5/LiTFSI in EMITFSI + PMMA/$Li_xWO_3.2H_2O$ device at −1.5 V for 60 s and 1.5 V for 60 s: (a) vanadium based side and (b) tungsten based side.